Local Geometry Inclusive Global Shape Representation

Somenath Das and Suchendra M. Bhandarkar
Department of Computer Science, The University of Georgia
Athens, Georgia 30602-7404, USA
somenath@uga.edu, suchi@cs.uga.edu

Abstract

A local geometry-inclusive global representation of 3D shapes based on the shortest quasi-geodesic paths between all possible pairs of points on the shape manifold is proposed. In the proposed representation, the normal curvature values along the quasi-geodesic paths are shown preserve the local shape geometry. The eigenspectrum of the proposed global representation is exploited to characterize the shape self-symmetry. The commutative property of the shape descriptor spectrum is exploited to address region-based correspondence determination between isometric 3D shapes without requiring prior correspondence maps and to extract stable regions between 3D shapes that differ from one another by a high degree of isometry transformation. Eigenspectrum-based characterization metrics are proposed to quantify the performance of the proposed 3D shape descriptor for correspondence determination and self-symmetry detection in comparison to its relevant state-of-the-art counterparts. The proposed shape descriptor spectrum and the optimization criterion based on spectral commutativity are observed to yield competitive performance compared to relevant state-of-the-art methods.

Keywords: 3D shape representation, eigenspectrum decomposition, shape correspondence, shape symmetry

1. Introduction

In the field of shape analysis, the computation of an optimal global description of a 3D shape is critically dependent upon the underlying application. Applications based on shape similarity computation typically rely on a suitably formulated global metric to characterize shape similarity. On the other hand, local shape geometry is important for applications where it is essential to establish point-to-point correspondence between candidate shapes. Based on the objective(s) of the application and nature or modality of the underlying shape data/information (i.e., geometric, topological, etc.), 3D shape analysis applications can be broadly categorized as purely geometric, semantic or knowledge-driven [1]. However, a large number of 3D shape analysis applications that belong to these categories or lie within their intersections are compelled to address a fundamental problem, i.e., that of determining accurate correspondence between the 3D shapes under consideration. Typical examples of such applications include rigid and non-rigid shape registration [2, 3], shape morphing [4], self-symmetry detection [5], shape deformation transfer [6], 3D surface reconstruction [7], shape-based object recognition and retrieval [8], to name a few. In each of the aforementioned applications, shape descriptors play a critical role in determining the required 3D shape correspondence. Depending on the nature of the application, 3D shape descriptors could be purely geometric and used to capture the *local* 3D geometry of the shapes whereas others may incorporate prior knowledge about the *global* 3D shape. Ideally, a 3D shape descriptor should demonstrate robustness to topological noise while simultaneously capturing the underlying invariant shape features that are useful in computing the correspondence between 3D shapes.

In this paper, we address an important problem, i.e., that of determining correspondence between isometric 3D shapes (i.e., 3D shapes that have undergone isometry deformation or transformation with respect to each other) *without* requiring any prior knowledge about the underlying shapes. To this end, we propose a 3D shape descriptor based on estimation of the approximate geodesic distance between all point pairs on the 3D shape manifold. The proposed representation is used to address the computation of 3D self-symmetry, determination of correspondence between isometric 3D shapes and detection of the most stable parts of the 3D shape under varying degrees of isometry (i.e, non-rigid pose) transformation between shapes. Since the geodesics over a 3D shape manifold are defined as surface curves of constant normal curvature, they are observed to naturally encode the local surface geometry along the curve. On a discrete triangulated 3D surface mesh, the discrete approximation to a geodesic is characterized by an optimal balance of the distribution of angles on either side of the discrete geodesic computed over the local neighborhood of

each mesh point on the geodesic as depicted in Figure 2. This balance of the local angular distribution is observed to encode the local geometry of the triangulated mesh along the discrete geodesic. The aforementioned approximation to a geodesic computed over a discrete 3D triangulated mesh is referred to as a *quasi-geodesic* [9]. The proposed global shape descriptor represents the 3D shape by computing the quasi-geodesic paths between all point pairs on the discrete 3D triangulated surface mesh.

The all-point-pairs geodesic matrix representation of 3D shapes displays a symmetrical pattern as shown in Figure 1. We employ the eigenspectrum of this representation to detect self-symmetry within a shape. Furthermore, we investigate the commutative property of the eigenvectors of the shape descriptor spectrum, which are shown to be approximately orthogonal to each other, for discrete settings such as the triangulated mesh-based representations of 3D shapes. Approximate orthogonality refers to the fact that for two distinct eigenvectors of the shape descriptor spectrum ϕ_i and ϕ_j (where $i \neq j$), $|\langle \phi_i, \phi_j \rangle| < \epsilon$ where $\langle \cdot, \cdot \rangle$ denotes the scalar inner product of the vector arguments and $\epsilon \approx 0$. It should be noted that the eigenspectrum of the proposed representation is distinct from the well known Laplace-Beltrami eigenspectrum that has been used extensively in several 3D shape analysis and 3D shape synthesis applications. In our case, we exploit the commutative property of the shape descriptor eigenspectrum to establish the correspondence between isometric 3D shapes. It should also be emphasized that, unlike many related approaches [10, 11], the proposed optimization criterion used to establish the correspondence between isometric 3D shapes does not exploit nor require prior user-specified correspondence maps between the 3D shapes.

We use the proposed correspondence optimization scheme to test the hypothesis that the presence of implicit isometry between 3D shapes can be characterized using a global quasi-geodesic-based shape representation that encodes local shape geometry. Furthermore, we also contend that the proposed representation can be exploited to address problems such as self-symmetry detection and characterization, correspondence determination and stable part or region detection under isometry deformation without resorting to prior knowledge of correspondence maps. To the best of our knowledge, the problem of correspondence determination in the absence of prior knowledge had not been addressed in the research literature. In some of our experiments, we obtain poor results for correspondence determination as a consequence of not requiring any prior knowledge in the face of high variability in the isometry transformations. However, our experiments show that the proposed correspondence determination technique is able to detect stable corresponding parts or regions between shapes, i.e., corresponding parts or regions that have undergone the least degree of isometry deformation (Section 5).

The remainder of the paper is organized as follows. In Section 2, we present a brief survey of the most relevant works on 3D shape description that can be effectively used to address 3D shape correspondence determination with an added emphasis on related work on coupled quasi-harmonic bases by Kovnatsky et. al. [10]. Section 3 describes the specific contributions of our work. The mathematical model on which the proposed technique is based is detailed in Section 4. In Section 5, we present the experimental results for 3D self-symmetry detection and characterization, 3D correspondence determination between isometric shapes, and stable 3D part or region detection. We conclude the paper in Section 6 with an outline of directions for future work.

2. Related Work and Background

The proposed global shape descriptor is based on the computation of quasi-geodesics between all pairs of points over the discrete triangulated 3D surface mesh that can encode the local geometry at discrete points over the surface mesh as well. The eigenspectrum of the descriptor is exploited to address shape self-symmetry and correspondence determination between isometric shapes. In this section, we first present a brief survey of relevant local shape representation schemes and spectrum-based shape correspondence models [12, 1]. We also discuss relevant work on coupled quasi-harmonic bases [10], which exploits the commutativity of the isometric shape eigenspectrum to establish correspondence between approximately isometric shapes.

2.1. Local shape descriptors

The different classes of local shape descriptors can be categorized based on their approach towards sampling of the underlying local surface geometry. **Ring-based descriptors** are typically based on local sampling of a predefined metric over the discrete 3D surface mesh, however, they differ in their strategies for evaluation of the metric. Some of the prominent descriptors belonging to this class employ *blowing bubbles* [13, 14] centered around a sample surface point, whereas others use the geodesic diameter to sample the surface metric in a local neighborhood [14]. These descriptors explicitly control the radius parameter of the bubbles or discs which in turn determines the size of the sample surface region.

Some ring-based descriptors [15] use the local surface normal vectors computed at discrete points on the surface mesh to capture the local surface features. *Geodesic fan descriptors* [15, 16] sample a local surface metric based on the values of the local surface curvature or the outward surface normal vector within regions of varying radii defined over the 3D surface mesh. *Splash descriptors* employ values of the surface normal vector as the primary metric for local surface characterization [17] whereas *point descrip-*

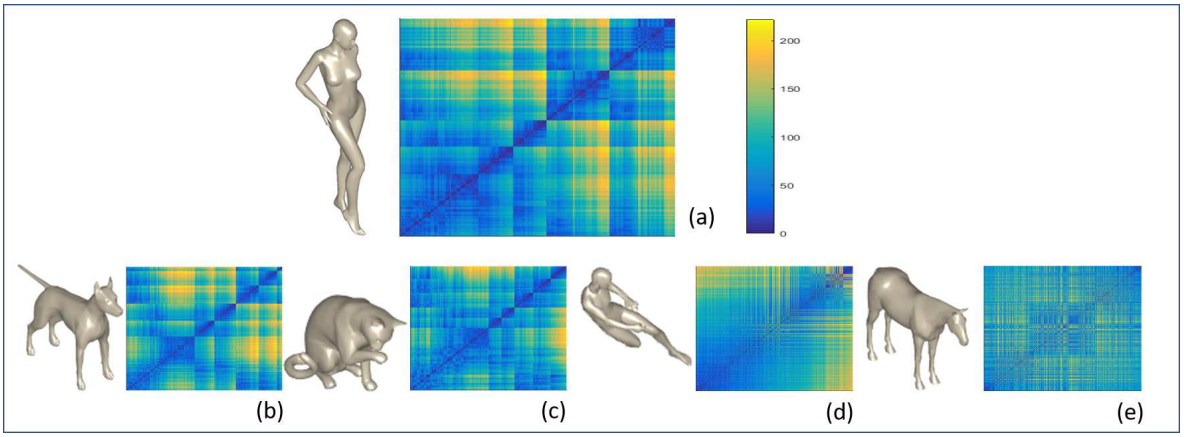

Figure 1. Global representation of 3D shapes using quasi-geodesics computed over a discrete triangulated 3D surface mesh. The 3D shape models shown are (a) *Victoria* (b) *Dog* (c) *Cat* (d) *Michael* and (e) *Horse*. The all-point-pairs quasi-geodesic matrix representation of the 3D shapes is observed to be approximately symmetric and the resulting eigenspectrum is observed to preserve self-symmetry over the discrete triangulated 3D mesh-based representation of the 3D shapes.

tors [18, 19, 20] encode the local geometric features on the surface mesh defined by the relative local surface normal at a sample point with respect to a superimposed plane or line segment at the sample points. One of the more prominent examples from this category of shape descriptors is the point descriptor proposed by Kokkinos et al. [21] where feature points are represented by local geometric and photometric fields.

Expanding descriptors fit a hypothesis-based model to a surface region in order to characterize it. Important shape descriptors from this category typically employ a parametric model involving features such as geodesic distance [22, 13], volume and/or surface area [23, 24]. Some variants of this descriptor use a mesh smoothing [25] or mesh saliency computation [26] procedure that is employed over a specific region on the 3D surface mesh.

Iterative operator-based descriptors capture the geometric changes within a shape by manipulating the entire mesh surface. As a manipulation strategy they employ techniques such as smoothing [25] or estimation of local diffusion geometry [27] over the mesh surface. The well known Laplace-Beltrami operator [28] is typically employed to compute the diffusion-based shape descriptors within this class.

2.2. Global shape representation

In most situations, knowledge of local surface geometry alone is insufficient to characterize the entire shape. Consequently, a global shape representation based upon local surface features is necessary to effectively address the correspondence problem, which is fundamental to many computer vision and computer graphics applications. In recent times, surface descriptors based on the eigenspectrum of the Laplace-Beltrami operator have gained popularity in the context of the correspondence problem. Some well known examples of surface descriptors from this class are based on the formulation of a diffusion process. The diffusion process is guided by the Laplace-Beltrami operator [28] that samples a surface metric, such as the mesh connectivity, along the geodesic curves on the 3D surface mesh. In related work, Bronstein et al. [27] use diffusion geometry to measure the point-to-point length along a specific path on the surface mesh using a random walk model.

Surface descriptors based on the *heat kernel signature* (HKS) [29, 30] employ the heat diffusion model in conjunction with the eigenspectrum of the Laplace-Beltrami operator to characterize global shape. In an anisotropic variation, Boscaini et al. [31] use the eigenspectrum of a directional version of the Laplace-Beltrami operator for shape representation. The *wave kernel signature* (WKS) [32] is another popular category of shape descriptors based on the Laplace-Beltrami eigenspectrum, that employs the principles of quantum mechanics instead of heat diffusion to characterize the shape. Smeets et al. [33] address the global representation of shape by computing the geodesic distances between sample points on the 3D surface mesh resulting in a shape representation scheme that is shown to achieve robustness against nearly isometric deformations. The level set-based deformable shape model [34], a variant of the diffusion-based shape descriptor, has been successfully employed in various applications such as surface segmentation, surface registration and object tracking.

2.3. Joint diagonalization of the commutative eigenspectrum

Point- or region-specific correspondence between isometric shapes can be addressed by exploiting the commutative property of the shape spectrum representation. In this section we briefly describe the technique by laying emphasis on relevant work on coupled quasi-harmonic bases [10] that employs the commutative property of the isometric (or near isometric) shape spectrum to address the problem of correspondence determination between isometric shapes.

2.3.1 Commutative eigenspectrum

Formally, the commutative property implies that given two unitary (i.e., Hermitian or orthogonal) operators Φ_X and Φ_Y defined over an isometric pair of shapes X and Y, one can determine a joint diagonalizer Ψ that diagonalizes both $\Psi^T\Phi_X\Psi$ and $\Psi^T\Phi_Y\Psi$ [35]. The joint diagonalizer Ψ represents the common eigenbases between the isometric shape spectra Φ_X and Φ_Y. Shapes represented as discrete triangulated meshes need not be exactly isometric to each other due to discretization error. Therefore, in the discrete case, the corresponding shape spectra would be *approximately commutative*. In this paper, the term *approximately commutative* is used in the following sense: The spectra Φ_X and Φ_Y of the triangulated shapes X and Y are approximately commutative if $||\Phi_X\Phi_Y - \Phi_Y\Phi_X||_F \approx 0$ where $||\Lambda||_F$ represents the Frobenius norm of matrix Λ.

A detailed treatment of the common eigenbases for approximately commutative spectral operators can be found in [35, 36]. Some recent important works [37, 10] employ the commutative principle to formulate a least-squares optimization criterion which is then used to extract a common spectral bases to address the problem of correspondence determination between isometric shapes. In the following subsection, we specifically describe the coupled quasi-harmonic bases formulated by Kovnatsky et. al. [10].

2.3.2 Coupled quasi-harmonic bases

The coupled quasi-harmonic bases address the problem of correspondence determination between two approximately isometric 3D shapes X and Y by determining the common bases that exist within their respective eigenspectra. The proposed optimization criterion determines bases $\widehat{\Phi}_X$ and $\widehat{\Phi}_Y$ that jointly diagonalize the Laplacians Δ_X and Δ_Y defined over the approximately isometric 3D shapes X and Y respectively. The common eigenbases $\widehat{\Phi}_X$ and $\widehat{\Phi}_Y$ are extracted via minimization of the optimization criterion in eqn. (1).

$$\begin{aligned}\underset{\widehat{\Phi}_X,\widehat{\Phi}_X}{\operatorname{argmin}} \Big\{ &\operatorname{off}(\widehat{\Phi}_X^T W_X \widehat{\Phi}_X) + \operatorname{off}(\widehat{\Phi}_Y^T W_Y \widehat{\Phi}_Y) + \\ &||F^T\widehat{\Phi}_X - G^T\widehat{\Phi}_Y||_F^2 \Big\} \\ \text{such that } &\widehat{\Phi}_X^T D_X \widehat{\Phi}_X = I \text{ and } \widehat{\Phi}_Y^T D_Y \widehat{\Phi}_Y = I\end{aligned} \tag{1}$$

In eqn. (1), $\operatorname{off}(A) = \sum_{1\le i\ne j\le n} |a_{ij}^2|$ for an $n \times n$ matrix A with elements a_{ij}. Matrices W and D are components of the discrete cotangent Laplacians Δ_X and Δ_Y of the discrete surface meshes X and Y respectively such that $\Delta_X = W_X^{-1}D_X$ and $\Delta_Y = W_Y^{-1}D_Y$. The cotangent discretization scheme for the mesh-based Laplacian proposed by Meyer et. al. [38] is used to compute the values of Δ_X and Δ_Y. The third term in the optimization criterion (eqn. (1)) represents the coarse correspondence between the 3D shapes X and Y provided that prior knowledge of the point-wise mapping between the shapes X and Y is stored in matrices F and G.

In this paper, we employ the principle of common eigenbases between shape spectrum corresponding to isometric shapes to establish region wise correspondence. However, in contrast to the coupled quasi-harmonic bases [10] described is eqn. (1), the optimization criterion proposed in the paper does not require any prior knowledge of the correspondence between the shapes under consideration. We further elaborate upon the optimization scheme for correspondence determination in Section 4.2.

3. Contributions of the Paper

In this paper, we propose a global shape representation $D_g(X)$ for a 3D manifold X that incorporates local surface geometry. The proposed representation is based on the computation of the shortest quasi-geodesic distances between all point pairs on the shape manifold. The proposed shape representation is shown to preserve the local surface geometry at each point on the 3D surface mesh. Furthermore, we effectively exploit the eigenspectrum of the proposed shape representation in the following applications:

(1) *Self-symmetry characterization*: We address the problem of self-symmetry characterization by exploiting the eigenspectrum of the proposed global shape descriptor $D_g(X)$.

(2) *Correspondence determination*: We determine the region-wise correspondence between isometric 3D shapes without requiring the user to determine and specify *a priori* the point-wise mapping between the two 3D shapes.

(3) *Isometry deformation characterization*: We exploit the results of the region-wise correspondence to characterize and quantify the extent of isometry deformation between the 3D shapes.

(4) *Stable part or region detection:* We exploit the commutative property of the eigenfunctions of $D_g(X)$ to extract

pose-invariant stable parts or surface regions within non-rigid 3D shapes under high degree of isometry transformation.

4. Local Geometry Inclusive Shape Operator

In the proposed scheme, a discrete 3D shape manifold X is characterized by an operator $D_g(X)$, that is computed by determining the quasi-geodesics over the discrete manifold X. It is known that along a geodesic over a continuous manifold, only the normal component of the local curvature is dominant when compared to the tangential component. A discrete 3D shape manifold X, in the form of a triangulated 3D surface mesh, can be represented by a C^2 differentiable function $f : \mathbb{R}^3 \rightarrow \mathbb{R}$ as $X = \{f(x_1), f(x_2), ..., f(x_n)\}$ where n denotes the number of vertices $x_i, 1 \leq i \leq n$ of X [39, 40]. The quasi-geodesic computed for a discrete path $x_i \rightsquigarrow x_j$ minimizes the distance measure $d(f(x_i), f(x_j))$ between the vertices x_i and x_j of X. The proposed shape representation $D_g(X)$ records all such quasi-geodesics, computed between all vertex-pairs or point-pairs over the surface mesh X. Furthermore, the matrix representation of $D_g(X)$ reveals an implicit symmetrical form, as is evident for the example 3D shapes shown in Figure 1.

For discrete meshes, the computation of geodesics is enabled by stable schemes such as the ones described in [9]. The local geometry along a quasi-geodesic over a discrete mesh is preserved as follows: Figure 2 depicts two scenarios where a probable quasi-geodesic (marked in red) crosses a neighborhood of triangular meshes. In either case, one can measure the discrete geodesic curvature at a point P as follows:

$$\kappa_g(P) = \frac{2\pi}{\theta}(\frac{\theta}{2} - \theta_r) \tag{2}$$

In eqn. (2), θ denotes the sum of all angles incident at point P where the geodesic crosses the surface mesh. In both cases, depicted in Figures 2(a) and 2(b), the quasi-geodesics generate angular distributions θ_l and θ_r such that $\theta_l = \sum_i \beta_i$ and $\theta_r = \sum_i \alpha_i$. Since the normal curvature is dominant along the quasi-geodesics, we can compute an optimum balance between θ_l and θ_r that minimizes the discrete geodesic curvature κ_g, which is the tangential curvature component along the quasi-geodesic. This optimal balance between angular distributions along the quasi-geodesic approximately encodes the local angular distribution and hence, the local geometry at surface point P as depicted in Figures 2(a) and 2(b).

The spectral decomposition of the symmetric shape operator $D_g(X)$ results in the eigenspectrum Φ_X for shape X as follows:

$$D_g(X)\Phi_X = \Delta_X \Phi_X \tag{3}$$

where $\Delta_X = \text{diag}(\gamma_1, \gamma_2, ..., \gamma_n)$ denotes the diagonal matrix of eigenvalues $\gamma_i, 1 \leq i \leq n$ and $\Phi_X = \{\Phi_X^1, \Phi_X^2, ..., \Phi_X^n\}$ denotes the eigenvectors $\Phi_X^i, 1 \leq i \leq n$ of shape X with n surface vertices.

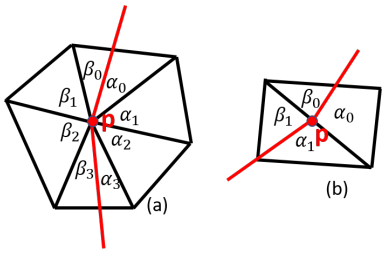

Figure 2. The right and left angular distributions θ_l and θ_r generated by a geodesic at point P on the surface mesh. The angular measures θ_l and θ_r encode the local geometry on a discrete surface mesh.

4.1. Self-symmetry characterization

We characterize self-symmetric regions over shape X as follows. Two regions $X_1, X_2 \subset X$ are possible candidates for being symmetric regions if for some upper bound ε:

$$\left| \sum_{k=1}^{k_0} \Phi_X^k(p) - \sum_{k=1}^{k_0} \Phi_X^k(q) \right|_2 \leq \varepsilon \quad \forall p \in X_1, \ \forall q \in X_2 \tag{4}$$

where $|\cdot|_2$ denotes the $\mathcal{L}^2$ norm. Using spectral analysis one can find a tight bound on ε such that $\varepsilon \leq \sum_{p,q \in X_1,\ r,s \in X_2} |d(p,q) - d(r,s)|_2$ for a C^2 distance metric d [41]. Parameter ε depends upon the variance of geodesic error computed over the entire shape manifold X. Therefore, for shape manifold X, ε is a measure of the degree of isometry deformation of X vis-a-vis the baseline shape. We report the bounds on ε computed for different meshes in the Experimental Results section (Section 5). For characterizing self-symmetry we restrict ourselves to the lower-order eigenvectors characterized by $k_0 \leq 20$. Furthermore, the above characterization can be also used to jointly analyze the correspondence between two candidate isometric shapes X and Y (Section 4.2).

4.2. Correspondence determination between isometric shapes

Determining the compatibility between the eigenbases of various shapes plays a critical role in applications dealing with analysis of multiple 3D shapes; in particular, determining the correspondence between 3D shapes. In related work, Ovsjanikov et al. [11] represent the correspondence between two shapes by a parametric map between their functional spaces. However, functional map-based methods typically rely on user-specified prior knowledge of the

mapping between the shapes for optimization of the correspondence criterion [42, 11]. In contrast, the proposed approach does not assume any user-specified prior mapping between the shapes under consideration.

For correspondence determination between two isometric shapes X and Y we exploit the fact that the eigendecomposition of symmetric shape operators $D_g(X)$ and $D_g(Y)$ leads to approximately commutative eigenspectra Φ_X and Φ_Y. The characterization "approximately commutative" is on account of the discretization or triangulation of the surface meshes describing the shapes and follows the formal definition given in Section 2.3. We couple Φ_X and Φ_Y by the commutative terms $\Phi_X^T \Delta_Y \Phi_Y$ and $\Phi_Y^T \Delta_X \Phi_X$ to solve the following optimization problem:

$$\bar{\Phi}_X, \bar{\Phi}_Y = \underset{\phi_x, \phi_y}{\operatorname{argmin}} \left\{ |\phi_x^T \Delta_Y \phi_y|_F + |\phi_y^T \Delta_X \phi_x|_F \right\} \quad (5)$$

where $\phi_x \subset \Phi_X$, $\phi_y \subset \Phi_Y$ and $|\cdot|_F$ denotes the Frobenius norm. It should be emphasized that eqn. (5) does not require that *a priori* correspondence maps be provided. The optimized maps $\bar{\Phi}_X$ and $\bar{\Phi}_Y$ over shapes X and Y encode the correspondence between them. From the optimized maps $\bar{\Phi}_X$ and $\bar{\Phi}_Y$, the relative correspondence error between shapes X and Y is given by $C_{X,Y} = \sum_{k=1}^{k_0} |\bar{\Phi}_X^k - \bar{\Phi}_Y^k|_2$. To compute $C_{X,Y}$ we consider the lower-order eigenvectors by setting $k_0 \leq 20$.

4.3. Stable 3D surface region or part detection

Relaxing the criterion for correspondence determination by not requiring a user-specified prior mapping between the shapes could result in poor correspondence between shapes that differ significantly from each other via isometry transformation. However, the optimization criterion for correspondence determination can also be used to identify common stable surface regions or parts within the shapes. These stable surface regions or parts are deemed to be the ones that have undergone the least amount of isometry deformation as a result of pose variation. We present the following criterion to identify the stable regions $S_{X,Y}$ between shapes X and Y as follows:

$$S_{X,Y} = \bigcup_p |\bar{\Phi}_X(p) - \bar{\Phi}_Y(p)|_2 \leq \varepsilon \quad (6)$$

where region p represents a corresponding region in both shapes X and Y identified by the correspondence optimization criterion in eqn. (5). The parameter ε is computed as mentioned in Section 4.1. The stable part detection is quantified using the following criterion: $\bar{S}_{X,Y} = \sum_{p \in S_{X,Y}} |\bar{\Phi}_X(p) - \bar{\Phi}_Y(p)|_2$.

5. Experimental Results

For our experiments we have chosen the TOSCA dataset consisting of ten non-rigid shape categories, i.e., *Cat*, *Dog*, *Wolf*, two *Human Males*, *Victoria*, *Gorilla*, *Horse*, *Centaur* and *Seahorse* [43]. Within each shape category, the individual shapes represent different transformations such as isometry, isometry coupled with topology change, different mesh triangulations of the same shape etc. In this work, we consider shapes that are isometric to one another, i.e., shapes that differ via an isometry transformation. Examples of some shapes that differ from one another via isometry transformations are shown in Figure 3. Experimental results are presented for six different shape categories for each of the applications formally described in Sections 4.1, 4.2 and 4.3 using visual representations of the results followed by the corresponding numerical evaluations. We have experimented with coarse meshes that are reduced by more than 87% of their original size or resolution. The results of the proposed shape representation are compared with those from relevant state-of-the-art shape representation schemes. The comparable performance achieved by the proposed local geometry-inclusive global shape representation scheme without requiring any prior knowledge of point-to-point or region-wise correspondences validates the central hypothesis underlying the proposed scheme, namely that the implicit isometry within candidate shapes can be exploited for correspondence determination without requiring that the knowledge of coarse correspondence be provided a priori.

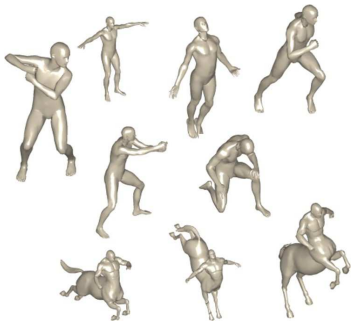

Figure 3. Examples of isometry transformation for the shape categories *Human Male* and *Centaur* in the TOSCA dataset.

5.1. Results of 3D self symmetry detection

Figure 4 depicts the self-symmetry maps obtained for the various shapes using eqn. (4). The maps in Figure 4 correspond to the second eigenvector Φ_X^2 obtained from the spectral decomposition of the global operator $D_g(X)$ for each shape using eqn. (3). Table 1 presents the self-symmetry characterization measure, denoted by the upper bound ε in eqn. (4), for each shape category. This characterization measure represents the average degree of isometry transformation within a shape category vis-a-vis the baseline shape. Note that the shape category *Michael* represents one of the two *Human Male* shape categories in the TOSCA dataset.

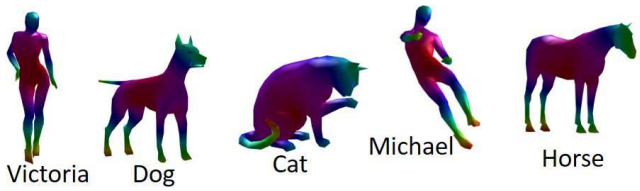

Figure 4. Self-symmetry detection for five different TOSCA shape categories using the spectrum of the global representation $D_g(X)$ for the shape X. Each map corresponds to the second eigenvector Φ_X^2 of the shape operator spectrum.

Table 1. Self-symmetry characterization measure for different shape categories in the TOSCA dataset. The average degree of isometry transformation within the category *Horse* is observed to be at least 30% higher than the other categories.

Category	ε	Category	ε
Victoria	0.528	*Dog*	0.462
Cat	0.282	*Michael*	0.566
Horse	0.815	*Centaur*	0.203

5.2. Results of 3D correspondence between isometric shapes

Since the lower-order eigenvectors represent global shape geometry more accurately, we consider the first 20 eigenvectors to compute the global region-based correspondence between the isometric shapes. Figure 5 shows the results of correspondence determination between the isometric *Human Male* shapes obtained via the optimization criterion described in eqn. (5). The correspondence maps between the shapes are shown to be consistent across the different order eigenvectors.

Table 2. Average relative error $C_{X,Y}$ in 3D correspondence determination between isometric shapes.

Category	Average $C_{X,Y}$	Category	Average $C_{X,Y}$
Victoria	0.069	*Dog*	0.0624
Cat	0.06	*Michael*	0.057
Horse	0.0559	*Centaur*	0.052

The relative correspondence error for these maps can be characterized by the measure $C_{X,Y}$ defined in Section 4.2. Table 2 lists this measure for isometric shapes from different TOSCA shape categories. Lower $C_{X,Y}$ values denote a higher degree of correspondence accuracy achieved via the optimization described in eqn. (5). We emphasize here, that the correspondence accuracy is achieved without requiring any user-specified prior mapping between the shapes.

5.3. Results of 3D stable region or part detection

Shapes from different categories display varying degrees of isometry transformations between them. As a result, the accuracy of global correspondence deteriorates for shapes that exhibit a very high degree of isometry deformation. This is expected since the proposed scheme does not assume any prior mapping information that could potentially improve the correspondence. However, using the criterion outlined in eqn. (6) we can identify the stable corresponding surface regions or parts within the shapes that are least transformed by isometry. The detected stable regions or parts for the *Centaur* shape category are depicted in Figure 6. For various poses of the *Centaur* shape model, the more dynamic regions such as the tail and the lower legs exhibit low correspondence accuracy and hence are rejected by the criterion described in eqn. (6). However, regions that are least affected by the isometry deformation are detected as stable regions. These stable regions exhibit high correspondence accuracy and are depicted in Figure 6. We quantify the correspondence accuracy for the detected stable regions using the measure $\bar{S}_{X,Y}$ described in Section 4.3. However, in our experiments, we observed a high positive correlation between the measures $C_{X,Y}$ and $\bar{S}_{X,Y}$. Hence we contend that the results in Table 2 hold for measure $\bar{S}_{X,Y}$ as well.

Table 3 compares the performance of the proposed representation scheme with the performance of other state-of-the-art representation schemes [44, 45]. The methods in [44, 45] were further combined with the functional map technique [11] in order to improve their correspondence accuracy via functional map-based local refinement. The results of performance comparison for these combined approaches with the proposed representation are also presented in Table 3. The numerical values presented in Table 3 denote the highest percentage correspondence accuracy achieved by the various representation schemes along with the corresponding average geodesic error. The performance of the proposed representation scheme is observed to compare very well with the performance of the other state-of-the-art representation schemes. These results underscore

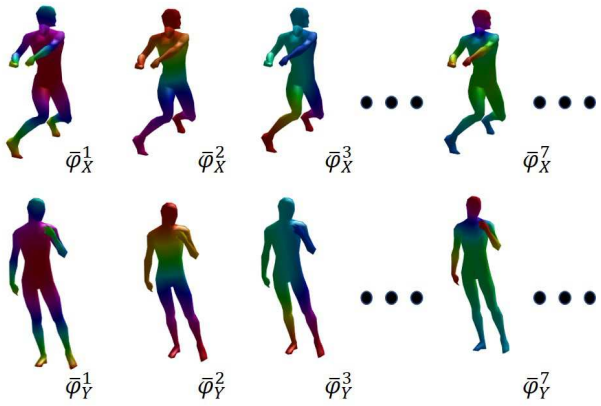

Figure 5. Pairwise consistency between corresponding eigenmaps of the *Human Male* shapes. For correspondence estimation, the optimization criterion described in eqn. (5) is used. Lower-order eigenvectors are considered for correspondence estimation since they effectively capture the global shape geometry.

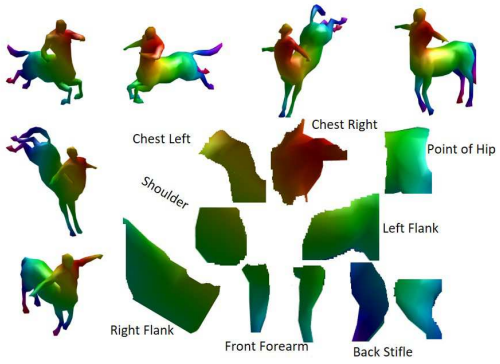

Figure 6. Stable region detection using the criterion outlined in eqn. (6). Stable surface regions are detected between isometric shapes where the correspondence accuracy is observed to deteriorate due to a high degree of isometry transformation between the shapes. Unstable regions are ones that exhibit a higher degree of isometry transformation between them, for example, parts of the lower legs, the tail, etc.

Table 3. Comparison between the proposed scheme and other state-of-the-art schemes described in Kim et al. [44], Sahillioglu and Yemez [45] and their combinations with Ovsjanikov et al. [11].

Methods	Geodesic Error	% Correspondence
[44]	0.11	~ 95
[11] and [44]	0.06	~ 95
[45]	0.25	~ 90
[11] and [45]	0.2	~ 90
Proposed Scheme	0.15	~ 94

the central hypothesis underlying the proposed shape representation, namely that competitive performance in self-symmetry detection and characterization, and correspondence map determination between isometric 3D shapes can be achieved by the proposed representation scheme without requiring prior knowledge of coarse correspondence mapping between the shapes unlike other state-of-the-art correspondence determination techniques [44, 45].

6. Conclusions and Future Work

In this paper we proposed a global shape representation scheme using quasi-geodesics computed over the entire discrete shape manifold. The eigenspectral decomposition of this representation is used effectively to identify self-symmetric regions on the discrete shape manifold. By exploiting the commutative property of the eigenbases of the proposed representation, we successfully demonstrated its use in correspondence determination between isometric shapes. We also proposed characterization metrics for self-symmetry identification and correspondence determination. Furthermore, stable surface regions within 3D shapes were identified for shape pairs that differed from each other by a high degree of isometry deformation. The results of correspondence determination obtained via the proposed representation scheme were compared with those from relevant state-of-the-art representation schemes.

A key contribution of this work is the fact that no prior knowledge, in the form of user-specified mappings, was used for correspondence determination and self-symmetry detection. As an extension of the current scheme, we intend to explore and combine functional maps [11] with the proposed representation that may prove critical in exploring the group structure within isometric shapes. Furthermore, we intend to use this combined scheme to address correspondence determination between near-isometric shapes [10].

References

[1] O. Van Kaick, H. Zhang, G. Hamarneh, and D. Cohen-Or, "A survey on shape correspondence," *Computer Graphics Forum*, vol. 30, no. 6, pp. 1681–1707, 2011. 1, 2

[2] W. Chang and M. Zwicker, "Automatic registration for articulated shapes," *Computer Graphics Forum*, vol. 27, no. 5, pp. 1459–1468, 2008. 1

[3] N. Gelfand, N. J. Mitra, L. J. Guibas, and H. Pottmann, "Robust global registration," *Symposium on Geometry Processing*, vol. 2, no. 3, p. 5, 2005. 1

[4] V. Kraevoy and A. Sheffer, "Cross-parameterization and compatible remeshing of 3D models," *ACM Transactions on Graphics (TOG)*, vol. 23, no. 3, pp. 861–869, 2004. 1

[5] R. Gal and D. Cohen-Or, "Salient geometric features for partial shape matching and similarity," *ACM Transactions on Graphics (TOG)*, vol. 25, no. 1, pp. 130–150, 2006. 1

[6] R. W. Sumner and J. Popović, "Deformation transfer for triangle meshes," *ACM Transactions on Graphics (TOG)*, vol. 23, no. 3, pp. 399–405, 2004. 1

[7] Y. Pekelny and C. Gotsman, "Articulated object reconstruction and markerless motion capture from depth video," *Computer Graphics Forum*, vol. 27, no. 2, pp. 399–408, 2008. 1

[8] V. Jain and H. Zhang, "A spectral approach to shape-based retrieval of articulated 3D models," *Computer Aided Design*, vol. 39, no. 5, pp. 398–407, 2007. 1

[9] D. Martínez, L. Velho, and P. C. Carvalho, "Computing geodesics on triangular meshes," *Computers & Graphics*, vol. 29, no. 5, pp. 667–675, 2005. 2, 5

[10] A. Kovnatsky, M. M. Bronstein, A. M. Bronstein, K. Glashoff, and R. Kimmel, "Coupled quasi-harmonic bases," *Computer Graphics Forum*, vol. 32, no. 2pt4, pp. 439–448, 2013. 2, 4, 8

[11] M. Ovsjanikov, M. Ben-Chen, J. Solomon, A. Butscher, and L. Guibas, "Functional maps: a flexible representation of maps between shapes," *ACM Transactions on Graphics (TOG)*, vol. 31, no. 4, p. 30, 2012. 2, 5, 6, 7, 8

[12] P. Heider, A. Pierre-Pierre, R. Li, and C. Grimm, "Local shape descriptors, a survey and evaluation," *Proceedings of the 4th Eurographics Conference on 3D Object Retrieval*, pp. 49–56, 2011. [Online]. Available: http://dx.doi.org/10.2312/3DOR/3DOR11/049-056 2

[13] M. Mortara, G. Patané, M. Spagnuolo, B. Falcidieno, and J. Rossignac, "Blowing bubbles for multi-scale analysis and decomposition of triangle meshes," *Algorithmica*, vol. 38, no. 1, pp. 227–248, 2004. 2, 3

[14] H. Pottmann, J. Wallner, Q.-X. Huang, and Y.-L. Yang, "Integral invariants for robust geometry processing," *Computer Aided Geometric Design*, vol. 26, no. 1, pp. 37–60, 2009. 2

[15] T. Gatzke, C. Grimm, M. Garland, and S. Zelinka, "Curvature maps for local shape comparison," *Proceedings of the International Conference on Shape Modeling and Applications*, pp. 244–253, 2005. 2

[16] J. Ong and A.-K. Seghouane, "From point to local neighborhood: Polyp detection in ct colonography using geodesic ring neighborhoods," *IEEE Transactions on Image Processing*, vol. 20, no. 4, pp. 1000–1010, April 2011. 2

[17] F. Stein and G. Medioni, "Structural indexing: Efficient 3-D object recognition," *IEEE Transactions on Pattern Analysis & Machine Intelligence*, no. 2, pp. 125–145, 1992. 2

[18] S. M. Yamany and A. A. Farag, "Free-form surface registration using surface signatures," *The Proceedings of the Seventh IEEE International Conference on Computer Vision*, vol. 2, pp. 1098–1104, 1999. 3

[19] C. S. Chua and R. Jarvis, "Point signatures: A new representation for 3D object recognition," *International Journal of Computer Vision*, vol. 25, no. 1, pp. 63–85, 1997. 3

[20] S. M. Yamany and A. A. Farag, "Surface signatures: an orientation independent free-form surface representation scheme for the purpose of objects registration and matching," *IEEE Transactions on Pattern Analysis and Machine Intelligence*, vol. 24, no. 8, pp. 1105–1120, 2002. 3

[21] I. Kokkinos, M. M. Bronstein, R. Litman, and A. M. Bronstein, "Intrinsic shape context descriptors for deformable shapes," *Proceedings of IEEE Conference on Computer Vision and Pattern Recognition (CVPR)*, pp. 159–166, 2012. 3

[22] G. Cipriano, G. N. Phillips, and M. Gleicher, "Multi-scale surface descriptors," *IEEE Transactions on Visualization and Computer Graphics*, vol. 15, no. 6, pp. 1201–1208, 2009. 3

[23] M. L. Connolly, "Measurement of protein surface shape by solid angles," *Journal of Molecular Graphics*, vol. 4, no. 1, pp. 3–6, 1986. 3

[24] H. Pottmann, J. Wallner, Q.-X. Huang, and Y.-L. Yang, "Integral invariants for robust geometry processing," *Computer Aided Geometric Design*, vol. 26, no. 1, pp. 37–60, 2009. 3

[25] X. Li and I. Guskov, "Multiscale features for approximate alignment of point-based surfaces." *Proceedings of Symposium on Geometry Processing*, vol. 255, pp. 217–226, 2005. 3

[26] C. H. Lee, A. Varshney, and D. W. Jacobs, "Mesh saliency," *ACM Transactions on Graphics (TOG)*, vol. 24, no. 3, pp. 659–666, Jul. 2005. [Online]. Available: http://doi.acm.org/10.1145/1073204.1073244 3

[27] A. M. Bronstein, M. M. Bronstein, R. Kimmel, M. Mahmoudi, and G. Sapiro, "A Gromov-Hausdorff framework with diffusion geometry for topologically-robust non-rigid shape matching," *International Journal of Computer Vision*, vol. 89, no. 2-3, pp. 266–286, 2010. 3

[28] R. M. Rustamov, "Laplace-Beltrami eigenfunctions for deformation invariant shape representation," *Proceedings of the Fifth Eurographics Symposium on Geometry Processing*, pp. 225–233, 2007. 3

[29] J. Sun, M. Ovsjanikov, and L. Guibas, "A concise and provably informative multi-scale signature based on heat diffusion," *Computer Graphics Forum*, vol. 28, no. 5, pp. 1383–1392, 2009. 3

[30] M. M. Bronstein and I. Kokkinos, "Scale-invariant heat kernel signatures for non-rigid shape recognition," *Proceedings of IEEE Conference on Computer Vision and Pattern Recognition (CVPR)*, pp. 1704–1711, 2010. 3

[31] D. Boscaini, J. Masci, E. Rodolà, M. M. Bronstein, and D. Cremers, "Anisotropic diffusion descriptors," *Computer Graphics Forum*, vol. 35, no. 2, pp. 431–441, 2016. 3

[32] M. Aubry, U. Schlickewei, and D. Cremers, "The wave kernel signature: A quantum mechanical approach to shape analysis," *Proceedings of IEEE International Conference on Computer Vision Workshops (ICCV Workshops)*, pp. 1626–1633, 2011. 3

[33] D. Smeets, J. Hermans, D. Vandermeulen, and P. Suetens, "Isometric deformation invariant 3D shape recognition," *Pattern Recognition*, vol. 45, no. 7, pp. 2817–2831, 2012. 3

[34] B. C. Lucas, M. Kazhdan, and R. H. Taylor, "Spring level sets: A deformable model representation to provide interoperability between meshes and level sets," *IEEE Transactions on Visualization and Computer Graphics*, vol. 19, no. 5, pp. 852–865, 2013. 3

[35] J.-F. cois Cardoso, "Perturbation of joint diagonalizers." 4

[36] A. Yeredor, "Non-orthogonal joint diagonalization in the least-squares sense with application in blind source separation," *IEEE Transactions on Signal Processing*, vol. 50, no. 7, pp. 1545–1553, 2002. 4

[37] A. Kovnatsky, M. M. Bronstein, X. Bresson, and P. Vandergheynst, "Functional correspondence by matrix completion," *Proceedings of the IEEE Conference on Computer Vision and Pattern Recognition (CVPR)*, pp. 905–914, 2015. 4

[38] M. Meyer, M. Desbrun, P. Schröder, and A. H. Barr, "Discrete differential-geometry operators for triangulated 2-manifolds," *Visualization and Mathematics III*, pp. 35–57, 2003. 4

[39] O. Azencot, S. Weißmann, M. Ovsjanikov, M. Wardetzky, and M. Ben-Chen, "Functional fluids on surfaces," *Computer Graphics Forum*, vol. 33, pp. 237–246, 2014. 5

[40] J. Martinez Esturo, C. Rössl, and H. Theisel, "Smoothed quadratic energies on meshes," *ACM Transactions on Graphics (TOG)*, vol. 34, no. 1, p. 2, 2014. 5

[41] N. Dunford and J. T. Schwartz, *Linear operators: Part II: Spectral Theory: Self Adjoint Operators in Hilbert Space*. Interscience Publishers, 1963. 5

[42] A. Nguyen, M. Ben-Chen, K. Welnicka, Y. Ye, and L. Guibas, "An optimization approach to improving collections of shape maps," *Computer Graphics Forum*, vol. 30, pp. 1481–1491, 2011. 6

[43] M. Ovsjanikov, A. M. Bronstein, M. M. Bronstein, and L. J. Guibas, "Shape Google: a computer vision approach to isometry invariant shape retrieval," pp. 320–327, 2009. 6

[44] V. G. Kim, Y. Lipman, and T. Funkhouser, "Blended intrinsic maps," *ACM Transactions on Graphics (TOG)*, vol. 30, no. 4, pp. 79:1–79:12, 2011. 7, 8

[45] Y. Sahillioglu and Y. Yemez, "Coarse-to-fine combinatorial matching for dense isometric shape correspondence," *Computer Graphics Forum*, vol. 30, no. 5, pp. 1461–1470, 2011. 7, 8